Available online at www.sciencedirect.com
ScienceDirect
Journal of Catalysis 247 (2007) 119–126
JOURNAL OF CATALYSIS
www.elsevier.com/locate/jcat

A DFT study of the mechanism and kinetics of methane oxidation to formaldehyde occurring on silica-supported molybdena

Shaji Chempath, Alexis T. Bell *

Department of Chemical Engineering, University of California, Berkeley, CA 94720-1462, USA

Received 14 September 2006; revised 10 January 2007; accepted 12 January 2007

Abstract

A theoretical analysis was carried out of the mechanism and kinetics of methane oxidation to formaldehyde occurring on isolated molybdate species supported on silica. Both mono-oxo and di-oxo molybdate structures were used to represent the active centers. The energetics for each elementary reaction was determined from density functional theory calculations, and the entropy changes were determined from calculations based on statistical mechanics. The results of this analysis show that the mechanism based on di-oxo molybdate species agrees more closely with observed rates of methane oxidation than that based on mono-oxo molybdate species. It is also found that the formation of formaldehyde occurs via the reaction of methane with peroxide species formed via the adsorption of O_2 on reduced Mo^{IV} centers. The extent of Mo^{VI} reduction to Mo^{IV} is well under 1% under reaction conditions, in good agreement with experimental observations.

Keywords: Quantum chemistry; Peroxide; MoO_x; Methane activation; CH_2O

1. Introduction

Silica-supported molybdena is known to be a highly active catalyst for the direct oxidation of methane to formaldehyde [1–7]. The effectiveness of silica is ascribed to the minimal decomposition of CH_2O on this material relative to other support oxides. It is also notable that for Mo surface concentrations below ∼1 Mo/nm^2, the turnover frequency for methane oxidation is independent of molybdena surface concentrations [2,4]. Because virtually all of the molybdena at such low surface densities is present as isolated molybdate species [8–17], this means that such species are active for the oxidation of methane to formaldehyde.

The mechanism and kinetics of methane oxidation to formaldehyde have been investigated by a number of authors [7,18–22]. In most of these studies, it is assumed that two O atoms, each associated with a single Mo atom, are involved in the formation of CH_2O and H_2O, and that reoxidation of the catalyst by O_2 restores one O atom per Mo. This sequence is represented by

$$CH_4 + 2Mo{=}O \rightarrow CH_2O + H_2O + 2Mo,$$
$$2Mo + O_2 \rightarrow 2Mo{=}O.$$

Although such simple schemes have been used successfully to describe the kinetics of methane oxidation [6,7,21], they are inconsistent with a number of physical observations. For example, the degree of reduction from Mo^{VI} to Mo^{IV} determined from such redox models of the mechanism is projected to be 10–20% [6,7], whereas experimental evidence suggests that the degree of reduction is <1% [22,23].

It is also difficult to understand how isolated molybdate species could catalyze the oxidation of CH_4 if O atoms from two completely isolated molybdate species are required. The incorporation of O atoms from molecular oxygen into reduced Mo sites is equally unexplained for this case. Further evidence against the formation of CH_2O via CH_4 reduction of Mo=O bonds associated with isolated molybdate species has come from pulse reaction studies [24]. Such experiments have shown that a pulse of CH_4 without O_2 reacts to a much smaller extent than does a pulse of CH_4 including O_2. The difference between the two experiments has been used to suggest that a metastable

* Corresponding author. Fax: +1 510 642 4778.
E-mail address: bell@cchem.berkeley.edu (A.T. Bell).

0021-9517/$ – see front matter
doi:10.1016/j.jcat.2007.01.012

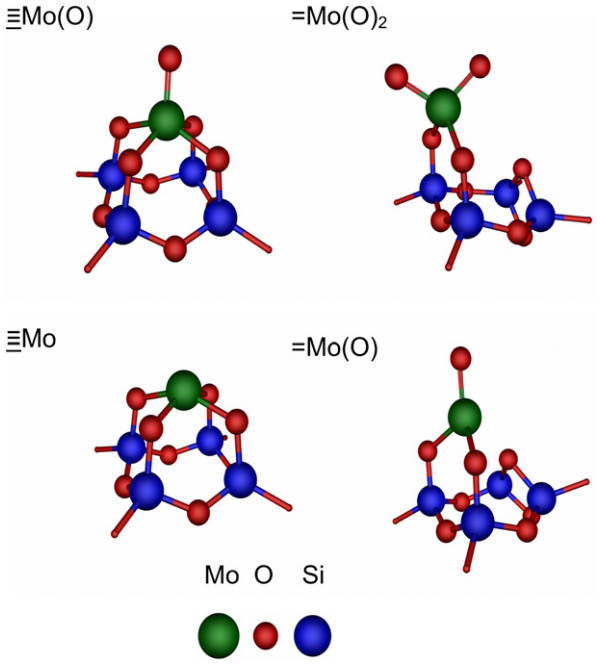

Fig. 1. Geometries of MoO_x anchored on silica. ≡Mo(O) and =$Mo(O)_2$ represent $Mo^{VI}O_x$ species while ≡Mo and =Mo(O) represent $Mo^{IV}O_x$ species.

form of oxygen exists that is incompletely reduced. This view is also supported by surface potential measurements [25,26] made under various CH_4 and O_2 partial pressures, which suggest that the form of oxygen involved in CH_4 oxidation is reduced by one electron per O atom. Building on these observations as well as their own, Ohler and Bell [22] proposed that CH_4 is oxidized by peroxide species formed by the reaction of O_2 with a small concentration of reduced molybdate species. In the first step of their mechanism, CH_4 adds across the peroxide to form an $Mo(OH)(OCH_3)$ species. Formaldehyde is then formed via the transfer of a hydrogen atom from the methoxide to the hydroxyl group. Desorption of formaldehyde and water lead to the final products.

Quantum mechanical investigations can provide information that is complementary to that obtained from experimental studies. Chempath et al. [27] recently reported a density functional theory (DFT) investigation of the structure of isolated molybdate species and compared their findings with experimental evidence obtained from Raman, XANES, and EXAFS observations [23]. They considered two possible modes of Mo^{VI} molybdate species bonded to silica: one with four Mo–O–Si linkages and another with two Mo–O–Si linkages. In the present paper, these modes are designated ≡Mo(O) and =$Mo(O)_2$, respectively (see Fig. 1). Their work demonstrated convincingly that isolated molybdate species are present as di-oxo, =$Mo(O)_2$, structures rather than mono-oxo, ≡Mo(O), structures after calcination of highly dispersed silica-supported molybdena (0.44 Mo/nm^2) at 920 K. H_2 reduction of =$Mo(O)_2$ was predicted to form =Mo(O), in good agreement with what has been observed experimentally by Raman and EXAFS.

Fu et al. [28] used DFT to examine the energetics of CH_4 oxidation using a Mo_3O_9 cluster to model supported MoO_x. In this model, each molybdenum has two Mo=O bonds and methane directly reacts with the Mo=O bonds to form a =$Mo(OH)(OCH_3)$ species, in which hydroxyl and methoxide groups are attached to the Mo(IV) cation. The overall free energy barrier at 873 K for direct methane activation by the Mo=O bonds is estimated to be 75.6 kcal/mol. The subsequent steps leading to formation of CH_2O and H_2O and the mechanism by which Mo^{IV} is reoxidized to Mo^{VI} were not considered.

The aim of the present investigation was to explore the plausibility of the reaction mechanism proposed by Ohler and Bell [22] for the oxidation of CH_4 to CH_2O occurring on isolated silica-supported molybdate species. Toward this end, DFT calculations were carried out using small molecular clusters to represent the elementary processes occurring on ≡Mo(O) and =$Mo(O)_2$. Particular attention was given to calculations of the thermodynamics of Mo^{VI} to Mo^{IV} reduction and the activation of methane by peroxide species formed by O_2 adsorption on structures containing Mo^{IV}. The equilibrium constants and rate coefficients determined in the course of this study were then used to predict the rate of methane oxidation for different temperatures and partial pressures of CH_4 and O_2. The ultimate goal of this work was to establish whether the overall rate of reaction occurring via ≡Mo(O) or =$Mo(O)_2$ is faster.

2. Theoretical methods

Silica-supported molybdate species were represented by the structures shown in Fig. 1. These models were chosen based on our previous study of the structure of MoO_x species on different cluster representations of a silica surface [27]. In that study, we found that an accurate representation of the energetics of Mo oxidation and reduction could be achieved using clusters containing four silicon atoms. Calculations with larger models gave similar energetics and vibrational frequencies to those obtained with the four-silicon model but at the expense of significantly higher computational time. For this reason, we have represented the surface of silica as a ring of four Si atoms connected together by four O atoms with the remaining valences of Si terminated by Si–OH groups. The Mo^{VI} molybdates were taken to be in the form of either mono-oxo [≡Mo(O)] or di-oxo [=$Mo(O)_2$]. Both structures are identical to those in our previous study. As noted in the Introduction, we recently showed that the Raman spectrum and EXAFS pattern of the di-oxo structure agree closely with those observed experimentally for isolated molybdate species supported on silica after calcination at 920 K [27]. The reason for considering both mono- and di-oxo structures in the present study is that our previous work has shown that these structures can co-exist, depending on the partial pressure of water and the temperature.

Electronic energies of reactant, product, and transition states were determined using DFT. The B3LYP functional was used to describe electron exchange and correlation. The geometry of ground-state and transition-state structures were optimized using the 6-31G* basis set. The LANL2DZ effective-core potential was used to describe the Mo atom. Molybdate species bonded to silica were treated as freestanding clusters. All of the atoms in the cluster were allowed to relax during the geome-

try optimizations, which were done using the Gaussian03 software [29]. The growing-string method developed by Peters et al. [30] was used to locate the minimum energy path that connects a reactant and product. This method does not require an initial guess for the reaction path. The point with highest energy on this reaction path is taken to be an initial guess for the transition state. This point was further converged to the exact saddle point by the Berny optimization algorithm as implemented in Gaussian03 software [29]. After a particular structure was optimized to a stationary point (transition state, or minimum energy structure), its energy was further refined by a calculation at a higher level of accuracy using the LACV3P**++ basis set, as implemented in the Jaguar software [31]. This calculation was done to take advantage of triple-zeta effective core potential basis set for molybdenum that is more accurate than the double zeta LANL2DZ basis set available in Gaussian03. All of the structures investigated in the present study are stable in the singlet state except for =Mo(O), which is more stable in the triplet state. Geometry-optimized =Mo(O) species in the triplet state are 16.6 kcal/mol lower in energy than in the singlet state with the same geometry.

Free energies of all structures were determined within the rigid-rotor, harmonic-oscillator approximation. The Hessian matrix required for such calculations was evaluated analytically by the Gaussian03 software with the 6-31G*/LANL2DZ basis set. Standard free energies were calculated by including translational, rotational, and vibrational partition functions. In reporting the energy change of reactions, ΔE designates the change in electronic energy with the zero point corrections, ΔG^0 designates the change in Gibbs free energy in the standard state, and ΔS^0 designates the change in entropy in the standard state. The activation barriers are represented as $\Delta E^{\ddagger}$, $\Delta G^{0,\ddagger}$, and $\Delta S^{0,\ddagger}$. Because the reaction rates were measured at 873 K [7,22], all calculations of thermodynamic properties reported in this paper were done at 873 K. The standard state for all species present in the gas phase was taken to be 1 atm. The standard state for molybdena species on the catalyst surface was taken to be a mole fraction of 1 (normalized by the total amount of molybdenum present).

The rate constant for each elementary step was estimated using absolute rate theory. Within the context of this theory, the rate coefficient is given by

$$k = \frac{k_b T}{h} \exp\left(-\frac{\Delta G^{0,\ddagger}}{RT}\right), \tag{1}$$

where k_b is Boltzmann's constant, T is the reaction temperature (873 K), h is Planck's constant, R is the universal gas constant, and $\Delta G^{0,\ddagger}$ is the Gibbs free energy of activation. The standard state for all of these calculations is $\theta_i = 1.0$ for all molybdenum-containing species, where θ_i is the fraction of all Mo in the form of the ith structure, and $P_i = 1.0$ atm, where P_i is the partial pressure of the ith gas-phase species. Equilibrium constants for all reactions were calculated using

$$K = \exp\left(-\frac{\Delta G^0}{RT}\right). \tag{2}$$

3. Results and discussion

Fig. 2 shows the proposed sequence of steps involved in the oxidation of CH_4 to CH_2O and H_2O, assuming that the reaction sequence starts with the mono-oxo molybdate ≡Mo(O). Values of ΔE, ΔS^0, ΔG^0, and K for each elementary step are given in Table 1, with the latter three quantities being evaluated at 873 K. Table 2 lists the values of $\Delta E^{\ddagger}$, $\Delta S^{0,\ddagger}$, $\Delta G^{0,\ddagger}$, and k for reactions 3a, 3b, and 4. Here again, $\Delta S^{0,\ddagger}$, $\Delta G^{0,\ddagger}$, and k are evaluated at 873 K. Rate coefficients for reactions 1 and 2 were not calculated, because these reactions reach equilibrium under steady-state reaction conditions (see Supplementary material). This scheme is very similar to that proposed by Ohler and Bell [22], with the exception that the reduction of ≡Mo(O) to ≡Mo is assumed to involve CH_4 rather than H_2. This choice of reductant was made because CH_4 is present as a majority component of the feed gas during CH_4 oxidation, whereas the concentration of H_2 is likely to be very small, because it is readily converted to H_2O.

Reaction 1 describes the reversible reduction of ≡Mo(O) by CH_4 to produce ≡Mo, as well as CH_2O and H_2O. As seen in Table 1, $\Delta G^0 = 28.5$ kcal/mol and $K = 7.0 \times 10^{-8}$ atm$^{1/2}$ at 873 K for this reaction. Therefore, the reduction of molybdate species by methane is expected to be quite limited, in good agreement with what has been observed experimentally [22]. The reversible adsorption of O_2 onto ≡Mo is described by reaction 2. The values of ΔG^0 and K for this reaction are −7.6 kcal/mol and 80 atm^{-1}, respectively, at 873 K. The reaction of CH_4 with ≡Mo(O_2) occurs in two stages. During the first stage (reaction 3a), one O atom of the peroxide inserts into a C–H bond of CH_4 to produce weakly associated CH_3OH. In the second stage (reaction 3b), CH_3OH reacts with the remaining O atom of the molybdate structure to form ≡Mo(OH)(OCH_3). A film clip of the progress of reactions 3a and 3b, along the minimum-energy pathway, is presented as Supplementary material. CH_2O is formed in reaction 4 via intramolecular transfer of an H atom from the methoxide group to the hydroxyl group of ≡Mo(OH)(OCH_3) to produce ≡Mo(H_2O)(CH_2O). Finally, desorption of CH_2O and H_2O are envisioned to occur via reactions 5 and 6, respectively. Rate coefficients for these two processes were not calculated, because they were found to be barrierless, and thus should be very rapid.

The mechanism shown in Fig. 3 is similar to that shown in Fig. 2, except that the reaction sequence begins with =Mo($O)_2$. Values of ΔE, ΔS^0, ΔG_0, and K for each elementary step are given in Table 3, with the latter three quantities evaluated at 873 K, and the values of $\Delta E^{\ddagger}$, $\Delta S^{0,\ddagger}$, $\Delta G^{0,\ddagger}$, and k for reactions 3a′, 3b′, and 4′ are listed in Table 4. As in the case for the mechanism presented in Fig. 2, rate coefficients for reactions 1′ and 2′ were not calculated, because these reactions reach equilibrium under steady-state reaction conditions. The value of ΔG^0 for reaction 1′ is 20.8 kcal/mol, which is significantly lower than that for reaction 1 (28.5 kcal/mol). Correspondingly, the value of K for reaction 1′ is two orders of magnitude higher than that for reaction 1 (6.2×10^{-6} atm$^{1/2}$ vs 7.0×10^{-8} atm$^{1/2}$); however, it is still small, and thus the extent of reduction of =Mo($O)_2$ will be low. The value of ΔG^0

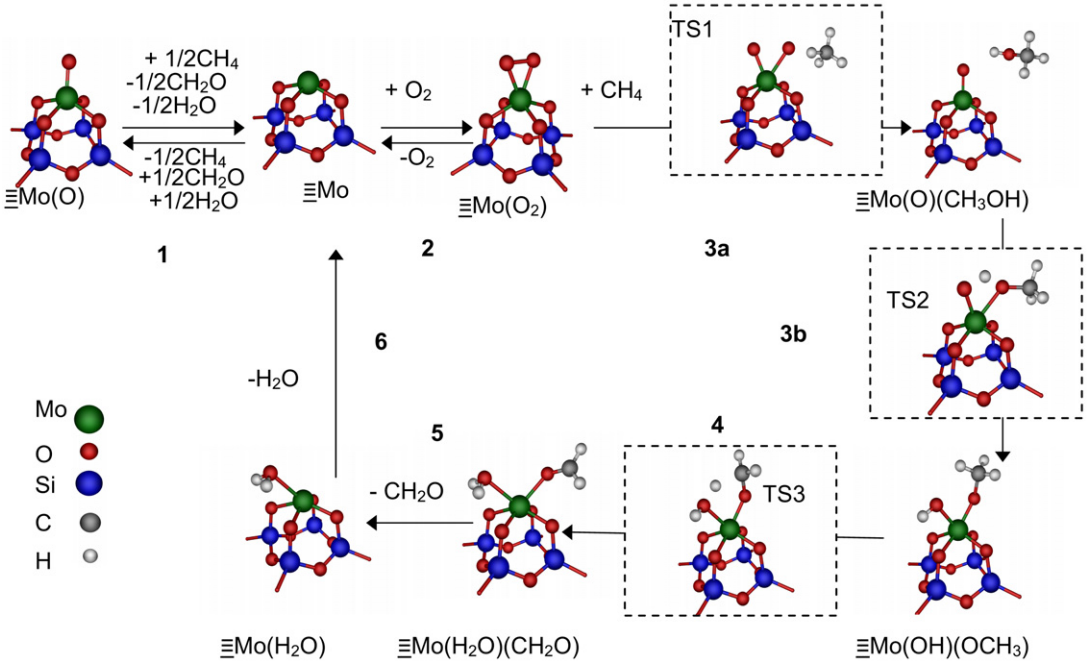

Fig. 2. Proposed reaction mechanism based on the assumption of ≡Mo(O) as the active center. Transition state structures are enclosed within dotted lines. Numbers in bold correspond to the reaction numbers shown in Tables 1 and 2.

Table 1
Changes in zero-point corrected energies, standard entropies and standard free energies at 873 K for the reaction cycle shown in Fig. 2

Reaction		ΔE (kcal/mol)	ΔS^0 (cal/mol/K)	ΔG^0 (kcal/mol)	K
$\equiv Mo(O) + 1/2CH_4 \leftrightarrow \equiv Mo + 1/2CH_2O + 1/2H_2O$	(1)	45.4	19.6	28.5	7.0×10^{-8}
$\equiv Mo + O_2 \leftrightarrow \equiv Mo(O_2)$	(2)	−40.3	−37.5	−7.6	80
$\equiv Mo(O_2) + CH_4 \rightarrow \equiv Mo(O)(CH3OH)$	(3a)	−64.7	−22.5	−45.0	1.8×10^{11}
$\equiv Mo(O)(CH_3OH) \rightarrow \equiv Mo(OH)(OCH_3)$	(3b)	15.6	−11.3	25.4	4.4×10^{-7}
$\equiv Mo(OH)(OCH3) \rightarrow \equiv Mo(H_2O)(CH_2O)$	(4)	0.8	+7.9	−6.0	32
$\equiv Mo(H_2O)(CH_2O) \rightarrow \equiv Mo(H_2O) + CH_2O$	(5)	13.0	32.6	−15.5	7.6×10^{3}
$\equiv Mo(H_2O) \rightarrow \equiv Mo + H_2O$	(6)	12.1	32.4	−16.2	1.1×10^{4}

Note. The last column shows the corresponding equilibrium constants.

Table 2
Activation energies, activation entropies, and activation free energy barriers at 873 K for the reaction cycle shown in Fig. 2

Reaction		$\Delta E^{\ddagger}$ (kcal/mol)	$\Delta S^{0,\ddagger}$ (cal/mol/K)	$\Delta G^{0,\ddagger}$ (kcal/mol)	k
$\equiv Mo(O_2) + CH_4 \rightarrow \equiv Mo(O)(CH_3OH)$	(3a)	27.3	−32.7	55.8	0.19 s^{-1} atm^{-1}
$\equiv Mo(O)(CH_3OH) \rightarrow \equiv Mo(OH)(OCH_3)$	(3b)	26.1	−14.1	38.3	4.7×10^{3} s^{-1}
$\equiv Mo(OH)(OCH_3) \rightarrow \equiv Mo(H_2O)(CH_2O)$	(4)	25.9	−4.5	29.8	6.3×10^{5} s^{-1}

Note. The last column shows the corresponding rate constants obtained with transition state theory.

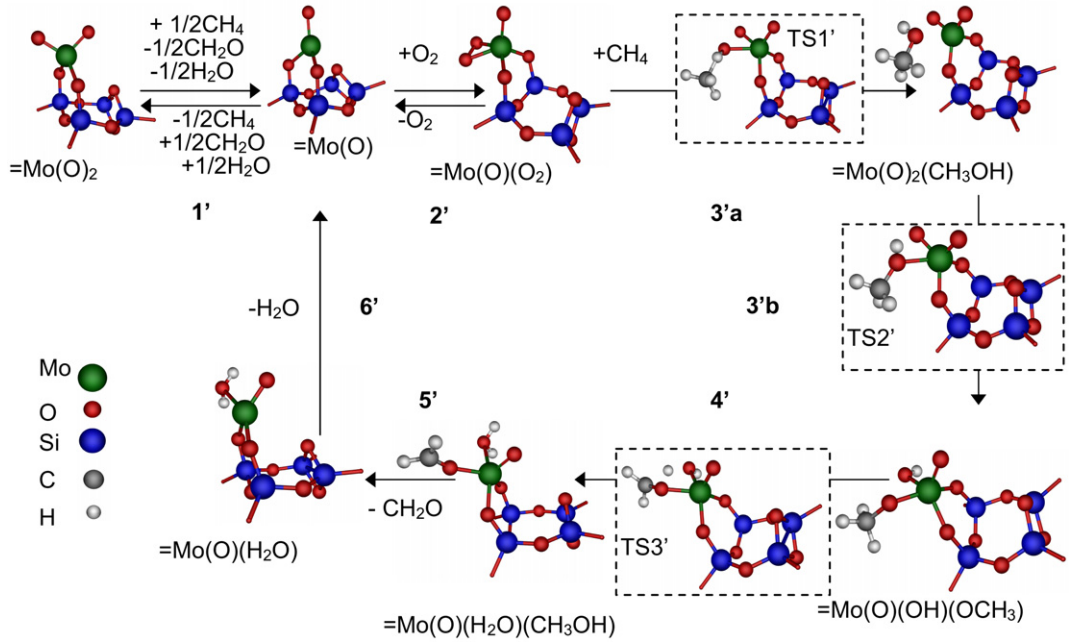

Fig. 3. Proposed reaction mechanism based on the assumption of $=Mo(O)_2$ as the active center. Transition state structures are enclosed within dotted lines. Numbers in bold correspond to the reaction numbers shown in Tables 3 and 4.

for reaction 2′ is somewhat smaller than that for reaction 2 (−8.7 kcal/mol vs −7.6 kcal/mol), and thus the value of K for reaction 2′ is larger than that for reaction 2 (150 atm^{-1} vs 80 atm^{-1}). Once the peroxide species, $=Mo(O)(O_2)$, is formed, the activation of methane (reactions 3a′ and 3b′) and the subsequent steps leading to CH_2O and H_2O (reactions 4′, 5′, and 6′) are qualitatively similar to the corresponding reactions shown in Fig. 2. Comparing Tables 2 and 4 shows, however, that the rate coefficients for reactions 3a′ and 3b′ are larger than those for reactions 3a and 3b. Rate coefficients for reactions 5′ and 6′ were not calculated, because here the reactions are barrierless as well.

A comparison of the energy and free energy profiles for the mechanisms presented in Figs. 2 and 3 is given in Fig. 4. For both cases, the energy or free energy is chosen to be zero once $\equiv Mo(O)$ or $=Mo(O)_2$ has been reduced to $\equiv Mo$ or $=Mo(O)$, respectively. It is evident from this figure that the elementary reaction with the largest free energy of activation is reaction 3a or reaction 3a′. The large values of $\Delta G^{0,\ddagger}$ for these reactions is a consequence of the large loss of entropy occurring on the adsorption of methane. For example, the entropic contribution to the free energy barrier at 873 K for reaction 3a′ is 29.6 kcal/mol.

Taking reaction 3a or 3a′ to be the rate-limiting step, the turnover frequency (TOF) for CH_2O formation can be written as

$$\mathrm{TOF} = k_{3a}\theta_{Mo(O_2)} P_{CH_4} \tag{3}$$

or

$$\mathrm{TOF} = k_{3a'}\theta_{Mo(O)(O_2)} P_{CH_4}, \tag{4}$$

where $\theta_{Mo(O_2)}$ and $\theta_{Mo(O)(O_2)}$ represent the fractions of Mo sites present as $\equiv Mo(O_2)$ and $=Mo(O)(O_2)$, respectively, and P_{CH_4} is the partial pressure of CH_4. As noted earlier, it can be shown that reactions 1 and 2, or reactions 1′ and 2′, will reach equilibrium under steady-state conditions. Consequently, $\theta_{Mo(O_2)}$ and $\theta_{Mo(O)(O_2)}$ can be written as

$$\theta_{Mo(O_2)} = K_1 K_2 \frac{P_{CH_4}^{1/2}}{P_{CH_2O}^{1/2} P_{H_2O}^{1/2}} P_{O_2} \theta_{Mo(O)} \tag{5}$$

or

$$\theta_{Mo(O)(O_2)} = K_{1'} K_{2'} \frac{P_{CH_4}^{1/2}}{P_{CH_2O}^{1/2} P_{H_2O}^{1/2}} P_{O_2} \theta_{Mo(O)_2}, \tag{6}$$

where $\theta_{Mo(O)}$ and $\theta_{Mo(O)_2}$ represent the fractions of Mo sites present as $\equiv Mo(O)$ and $=Mo(O)_2$, respectively, and P_{O_2} is the partial pressure of O_2. The mole fraction of $\equiv Mo(O)$ is evaluated to be >99% at steady state, implying that $\theta_{Mo(O)} \approx 1$. Similarly for the reaction network given in Fig. 3, $\theta_{Mo(O_2)}$ is evaluated to be very close to 1. Equations (1) and (2) now can be rewritten using Eqs. (5) and (6), together with the constraint that at high space velocities, $P_{CH_2O} = P_{H_2O}$ [7], and $\theta_{Mo(O)_2} \approx \theta_{Mo(O)} \approx 1$, to obtain

$$\mathrm{TOF} = k_{3a} K_1 K_2 \frac{P_{CH_4}^{3/2}}{P_{CH_2O}} P_{O_2} \tag{7}$$

or

$$\mathrm{TOF} = k_{3a'} K_{1'} K_{2'} \frac{P_{CH_4}^{3/2}}{P_{CH_2O}} P_{O_2}. \tag{8}$$

The rate expressions given by Eqs. (7) and (8) were compared with the experimental results reported by Ohler and Bell [7] at a temperature of 873 K, a total pressure of 1.14 atm, a CH_4 mole fraction of 0.9, a O_2 mole fraction of 0.1, a catalyst residence time of 0.38 s, and 3×10^{-4} mol Mo/g catalyst. For these

Table 3
Changes in zero-point corrected energies, standard entropies and standard free energies at 873 K for the reaction cycle shown in Fig. 3

Reaction		ΔE (kcal/mol)	ΔS^0 (cal/mol/K)	ΔG^0 (kcal/mol)	K
$=Mo(O)_2 + 1/2CH_4 \leftrightarrow =Mo(O) + 1/2CH_2O + 1/2H_2O$	(1′)	37.0	18.6	20.8	6.2×10^{-6}
$=Mo(O) + O_2 \leftrightarrow =Mo(O)(O_2)$	(2′)	−41.5	−37.5	−8.7	150
$=Mo(O)(O_2) + CH_4 \rightarrow =Mo(O)_2(CH_3OH)$	(3a′)	−65.0	−32.2	−36.9	1.7×10^9
$=Mo(O)_2(CH_3OH) \rightarrow =Mo(O)(OH)(OCH_3)$	(3b′)	0.01	−3.0	2.6	0.22
$=Mo(O)(OH)(OCH_3) \rightarrow =Mo(O)(H_2O)(CH_2O)$	(4′)	17.1	4.5	13.2	5.0×10^{-4}
$=Mo(O)(H_2O)(CH_2O) \rightarrow =Mo(O)(H_2O) + CH_2O$	(5′)	17.0	39.7	−17.6	2.5×10^4
$=Mo(O)(H_2O) \rightarrow =Mo + H_2O$	(6′)	8.7	30.2	−17.6	2.5×10^4

Note. The last column shows the corresponding equilibrium constants.

Table 4
Activation energies, activation entropies, and activation free energy barriers at 873 K for the reaction cycle shown in Fig. 3

Reaction		$\Delta E^{\ddagger}$ (kcal/mol)	$\Delta S^{0,\ddagger}$ (cal/mol/K)	$\Delta G^{0,\ddagger}$ (kcal/mol)	k
$=Mo(O)(O_2) + CH_4 \rightarrow =Mo(O)_2(CH_3OH)$	(3a′)	24.3	−33.9	53.9	0.58 s^{-1} atm^{-1}
$=Mo(O)_2(CH_3OH) \rightarrow =Mo(O)(OH)(OCH_3)$	(3b′)	22.2	−4.5	26.0	5.6×10^6 s^{-1}
$=Mo(O)(OH)(OCH_3) \rightarrow =Mo(O)(H_2O)(CH_2O)$	(4′)	27.3	−5.7	32.2	1.6×10^5 s^{-1}

Note. The last column shows the corresponding rate constants obtained with transition state theory.

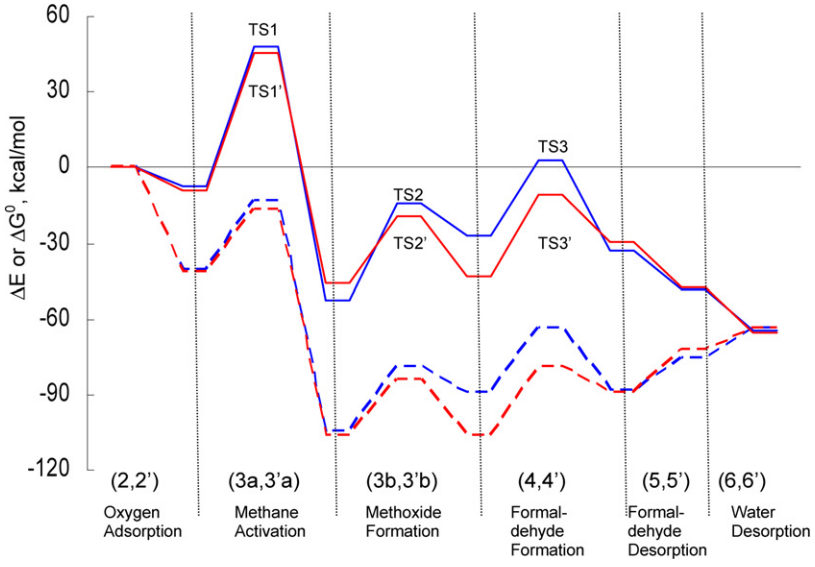

Fig. 4. Changes in energy (dashed lines) and free energy (solid lines) along the reaction pathway. The blue lines correspond to reaction mechanism starting with ≡Mo(O) (Fig. 2) and red lines correspond to reaction mechanism starting with $=Mo(O)_2$ (Fig. 3).

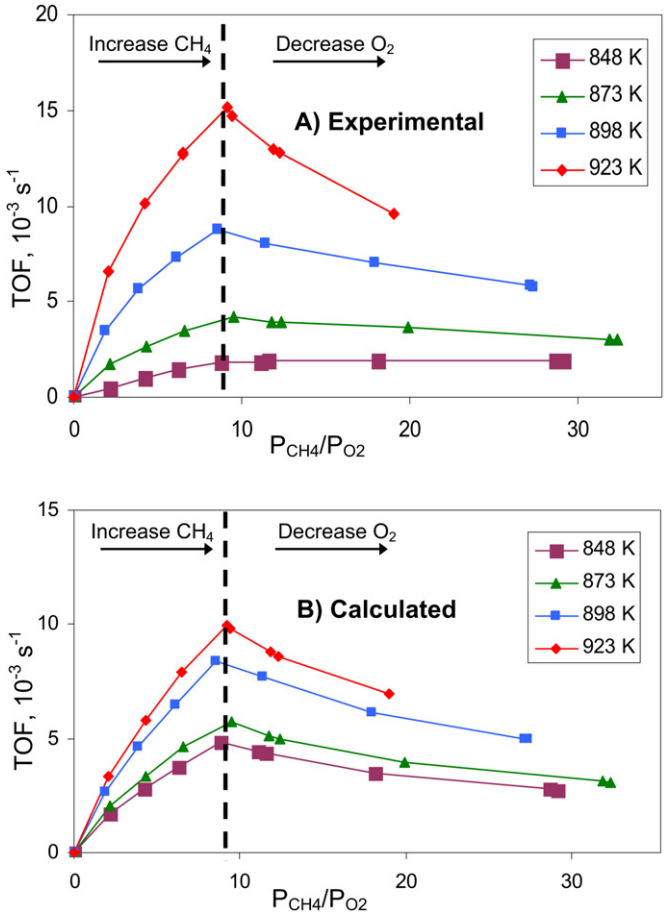

Fig. 5. Experimental (A) and calculated (B) TOFs for methane conversion at various temperatures. Ratio of methane to oxygen is varied by keeping the feed O_2 mole fraction constant at 10% and increasing the feed CH_4 mole fraction up to 90%, and then by keeping feed mole fraction of CH_4 constant at 90% and decreasing the feed O_2 mole fraction from 10% down to 2.7%.

conditions, the experimentally observed TOF for methane consumption is 4.2×10^{-3} s^{-1}. (Details of these calculations are given in Supplementary material.) When evaluating the TOF for methane consumption from Eqs. (7) and (8), it was assumed that the selectivity to CH_2O is 100%. The partial pressure of H_2O and CH_2O then can be calculated readily from a model for the reactor that assumes complete backmixing (a CSTR), because the conversion of methane is <6%. Working under these assumptions, the calculated TOF derived from Eq. (7) and the values given in Tables 1 and 2 is 2.7×10^{-4} s^{-1}, whereas that determined from Eq. (8) and the parameter values given in Tables 3 and 4 is 5.9×10^{-3} s^{-1}. If the experimentally observed selectivity to CH_2O (40%) is used, then the TOF values obtained from Eqs. (7) and (8) increase to 3×10^{-4} and 6.6×10^{-3} s^{-1}, respectively. These results show that only the model based on di-oxo molybdate species (shown in Fig. 3) is consistent with the experimentally measured TOF. These calculations also lead to the conclusion that at steady state, 210 ppm of the Mo^{VI} is reduced to Mo^{IV}, and the surface is covered by 3200 ppm of $=Mo(O)(O_2)$ (at 873 K, 90% CH_4, and 10% O_2). The very low level of Mo reduction is consistent with the observation by Raman spectroscopy that the state of the working catalyst is virtually identical to that of the fully oxidized catalyst [15,22].

As a further test of the reaction mechanism shown in Fig. 3 and the rate equation given by Eq. (8), a plot was made of the rate of methane consumption versus the partial pressures of CH_4 and O_2 in the feed for temperatures of 848, 873, 898, and 923 K (see Fig. 5). The experimental results of Ohler and Bell [7] are illustrated in panel A, and the calculated results are illustrated in panel B. The latter information is based on the assumption of 100% selectivity to CH_2O. The calculated dependences of the TOF for methane conversion on CH_4 and O_2 partial pressures are in good qualitative agreement with those seen experimentally. The observed differences are due in part to the assumption of 100% CH_2O selectivity in the calculations and in part to failure of the DFT calculations to fully capture the exact rates of elementary processes occurring at the catalytically active sites. Nevertheless, the level of agreement is sufficiently high to lend further support for the identity of the active site as di-oxo molybdate species and the reaction mechanism to be that shown in Fig. 3. We note that whereas the absolute values of the activation energies and heats of reaction may depend on the choice of density functional and basis set used, our experience shows that this will not affect the relative rates of reaction determined for the mechanisms shown in Figs. 3 and 4.

4. Conclusions

Two mechanisms have been proposed for the oxidation of methane to formaldehyde on isolated molybdate species supported on silica. The first of these (see Fig. 2) is based on the assumption that the active centers are mono-oxo molybdate species, ≡Mo(O), whereas the second mechanism (see Fig. 3) assumes that the active centers are di-oxo molybdate species, $=Mo(O)_2$. A theoretical analysis of the kinetics derived for both systems shows that the rate of methane consumption based on the second model is consistent with experimentally observed kinetics. An important finding of the present work is that the formation of formaldehyde is a result of methane reaction with an adsorbed peroxide species formed on reduced =Mo(O) centers. The present analysis is also shows that under reaction conditions the extent of Mo^{VI} reduction to Mo^{IV} is <1% consistent with the experimental observation.

Acknowledgment

This work was supported by the Methane Conversion Cooperative funded by BP.

Supplementary material

The online version of this article contains additional supplementary material.

A zip archive containing details of rate calculations, minimum energy geometries, and transition states is included. This archive contains an MS-WORD file that explains the TOF calculations and lists the catalyst details and operating condi-

tions used in the calculations. An MPEG movie showing the minimum-energy-path of the methane activation reaction by the peroxide is included in the archive. The archive also contains sub-directories with minimum energy structures in XYZ format and Gaussian03 output files of transition state calculations. README.txt files are included within the archive to guide the reader.

Please visit DOI: 10.1016/j.jcat.2007.01.012.

References

[1] A. Parmaliana, F. Arena, J. Catal. 167 (1997) 57.
[2] M.A. Bañares, J.L.G. Fierro, J.B. Moffat, J. Catal. 142 (1993) 406.
[3] A. Parmaliana, F. Frusteri, A. Mezzapica, M.S. Scurrell, N. Giordano, J. Chem. Soc. Chem. Commun. (1993) 751.
[4] M.A. Bañares, J.L.G. Fierro, ACS Symp. Ser. 523 (1993) 355.
[5] N.D. Spencer, C.J. Pereira, AIChE J. 33 (1987) 1808.
[6] F. Arena, A. Parmaliana, Acc. Chem. Res. 36 (2003) 867.
[7] N. Ohler, A.T. Bell, J. Catal. 231 (2005) 115.
[8] R.D. Roark, S.D. Kohler, J.G. Ekerdt, Catal. Lett. 16 (1992) 71.
[9] R.D. Roark, S.D. Kohler, J.G. Ekerdt, D.S. Kim, I.E. Wachs, Catal. Lett. 16 (1992) 77.
[10] M. Deboer, A.J. Vandillen, D.C. Koningsberger, J.W. Geus, M.A. Vuurman, I.E. Wachs, Catal. Lett. 11 (1991) 227.
[11] S. Takenaka, T. Tanaka, T. Funabiki, S. Yoshida, J. Phys. Chem. B 102 (1998) 2960.
[12] M.A. Bañares, H.C. Hu, I.E. Wachs, J. Catal. 150 (1994) 407.
[13] H.C. Hu, I.E. Wachs, S.R. Bare, J. Phys. Chem. 99 (1995) 10897.
[14] M. Faraldos, M.A. Bañares, J.A. Anderson, H.C. Hu, I.E. Wachs, J.L.G. Fierro, J. Catal. 160 (1996) 214.
[15] M.A. Bañares, N.D. Spencer, M.D. Jones, I.E. Wachs, J. Catal. 146 (1994) 204.
[16] M.A. Bañares, H.C. Hu, I.E. Wachs, J. Catal. 155 (1995) 249.
[17] C.C. Williams, J.G. Ekerdt, J.M. Jehng, F.D. Hardcastle, A.M. Turek, I.E. Wachs, J. Phys. Chem. 95 (1991) 8781.
[18] T.A. Garibyan, L.Y. Margolis, Catal. Rev. Sci. Eng. 31 (1989) 355.
[19] H.F. Liu, R.S. Liu, K.Y. Liew, R.E. Johnson, J.H. Lunsford, J. Am. Chem. Soc. 106 (1984) 4117.
[20] N.D. Spencer, C.J. Pereira, R.K. Grasselli, J. Catal. 126 (1990) 546.
[21] M.D. Amiridis, J.E. Rekoske, J.A. Dumesic, D.F. Rudd, N.D. Spencer, C.J. Pereira, AIChE J. 37 (1991) 87.
[22] N. Ohler, A.T. Bell, J. Phys. Chem. B 110 (2006) 2700.
[23] N. Ohler, A.T. Bell, J. Phys. Chem. B 109 (2005) 23419.
[24] A. Parmaliana, F. Arena, F. Frusteri, D. Miceli, V. Sokolovskii, Catal. Today 24 (1995) 231.
[25] Y. Barbaux, A. Elamrani, J.P. Bonnelle, Catal. Today 1 (1987) 147.
[26] Y. Barbaux, A.R. Elamrani, E. Payen, L. Gengembre, J.P. Bonnelle, B. Grzybowska, Appl. Catal. 44 (1988) 117.
[27] S. Chempath, Y. Zhang, A.T. Bell, J. Phys. Chem. C 111 (2007) 1291.
[28] G. Fu, X. Xu, X. Lu, H.L. Wan, J. Am. Chem. Soc. 127 (2005) 3989.
[29] M.J. Frisch, G.W. Trucks, H.B. Schlegel, G.E. Scuseria, M.A. Robb, J.R. Cheeseman, J.A. Montgomery Jr., T. Vreven, K.N. Kudin, J.C. Burant, J.M. Millam, S.S. Iyengar, J. Tomasi, V. Barone, B. Mennucci, M. Cossi, G. Scalmani, N. Rega, G.A. Petersson, H. Nakatsuji, M. Hada, M. Ehara, K. Toyota, R. Fukuda, J. Hasegawa, M. Ishida, T. Nakajima, Y. Honda, O. Kitao, H. Nakai, M. Klene, X. Li, J.E. Knox, H.P. Hratchian, J.B. Cross, C. Adamo, J. Jaramillo, R. Gomperts, R.E. Stratmann, O. Yazyev, A.J. Austin, R. Cammi, C. Pomelli, J.W. Ochterski, P.Y. Ayala, K. Morokuma, G.A. Voth, P. Salvador, J.J. Dannenberg, V.G. Zakrzewski, S. Dapprich, A.D. Daniels, M.C. Strain, O. Farkas, D.K. Malick, A.D. Rabuck, K. Raghavachari, J.B. Foresman, J.V. Ortiz, Q. Cui, A.G. Baboul, S. Clifford, J. Cioslowski, B.B. Stefanov, G. Liu, A. Liashenko, P. Piskorz, I. Komaromi, R.L. Martin, D.J. Fox, T. Keith, M.A. Al-Laham, C.Y. Peng, A. Nanayakkara, M. Challacombe, P.M.W. Gill, B. Johnson, W. Chen, M.W. Wong, C. Gonzalez, J.A. Pople, Gaussian 03 (Revision B.05), Gaussian, Inc., Pittsburgh, PA, 2003.
[30] B. Peters, A. Heyden, A.T. Bell, A. Chakraborty, J. Chem. Phys. 120 (2004) 7877.
[31] Jaguar 5.5, Schrödinger, LLC, Portland, OR, 1991–2003.